

1 Global source apportionment of aerosols into major emission regions  
2 and sectors over 1850–2017

3  
4  
5 Yang Yang<sup>1\*</sup>, Shaoxuan Mou<sup>1</sup>, Hailong Wang<sup>2</sup>, Pinya Wang<sup>1</sup>, Baojie Li<sup>1</sup>, Hong Liao<sup>1</sup>

6  
7  
8  
9 <sup>1</sup>Joint International Research Laboratory of Climate and Environment Change (ILCEC),  
10 Jiangsu Key Laboratory of Atmospheric Environment Monitoring and Pollution Control,  
11 Jiangsu Collaborative Innovation Center of Atmospheric Environment and Equipment  
12 Technology, School of Environmental Science and Engineering, Nanjing University of  
13 Information Science and Technology, Nanjing, Jiangsu, China

14 <sup>2</sup>Atmospheric, Climate, and Earth Sciences Division, Pacific Northwest National Laboratory,  
15 Richland, Washington, USA

16  
17  
18  
19  
20  
21 \*Correspondence to yang.yang@nuist.edu.cn

22 **Abstract**

23 Anthropogenic emissions of aerosols and precursor gases have been changing significantly in  
24 the past few decades across the world. In this study, an explicit aerosol source tagging system  
25 (EAST) is merged into the Energy Exascale Earth System Model version 1 (E3SMv1) to  
26 quantify the variations in anthropogenic aerosol concentrations, source contributions, and  
27 their subsequent radiative impact in four major emission regions on the globe during 1850–  
28 1980, 1980–2010 and 2010–2017. In North America and Europe, changes in anthropogenic  
29 PM<sub>2.5</sub> were mainly caused by changes in emissions from local energy and industrial sectors.  
30 The local industrial sector caused the most increase in PM<sub>2.5</sub> in East Asia during 1980–2010  
31 and decrease during 2010–2017. In South Asia, the increase in energy-related emissions  
32 dominated the rise of PM<sub>2.5</sub> levels during 1980–2017. During 1850–1980, the increases in  
33 emissions from North America contributed to the increase in European PM<sub>2.5</sub> burden by 1.7  
34 mg m<sup>-2</sup> and the sources from the Europe were also responsible for the PM<sub>2.5</sub> burden increase  
35 in East Asia and South Asia by about 1.0 mg m<sup>-2</sup>. During 1980–2010, East Asia contributed  
36 to an increase of 0.4–0.6 mg m<sup>-2</sup> in PM<sub>2.5</sub> burden in North America and Europe, while South  
37 Asian contributed about 0.3 mg m<sup>-2</sup>. During 2010–2017, the contributions from East Asia to  
38 the PM<sub>2.5</sub> burdens in the North America, Europe and South Asia declined by 0.3–0.6 mg m<sup>-2</sup>  
39 due to Clean Air actions in China, while the contributions from South Asia still increased due  
40 to the continuous increase in emissions in South Asia. The historical changes in aerosols had  
41 an impact on effective radiative forcing through aerosol-radiation interactions (ERF<sub>ari</sub>).  
42 During 1980–2010, a decline in North American aerosols resulted in a positive ERF<sub>ari</sub> change  
43 (warming effect) in Europe and a decline of aerosols in Europe caused a warming effect in

44 Russia and northern China. The changes in  $ERF_{ari}$  from the increase and decrease of aerosols  
45 in China during 1980–2010 and 2010–2017, respectively, are comparable in magnitude. The  
46 continuous aerosol increases in South Asia from 1980 to 2017 resulted in negative  $ERF_{ari}$   
47 (cooling) changes in South Asia, Southeast Asia, and southern China.

## 48 **1. Introduction**

49 Atmospheric aerosols, also known as particulate matter (PM), have significant influences  
50 on air quality and human health (Anenberg et al., 2010; Finlayson-Pitts and Pitts, 1997; Li et  
51 al., 2017; Pöschl, 2005). Aerosols also affect the energy budget of the earth system by  
52 scattering and/or absorbing solar radiation, thus directly affecting the climate (Gao et al., 2022;  
53 Yang et al., 2020a, 2023; Wang et al., 2023). Meanwhile, they may act as cloud condensation  
54 nuclei and/or ice nuclei, changing cloud characteristics and atmospheric water cycle, which  
55 indirectly affect the climate (Liao et al., 2015; Lohmann and Feichter, 2005; Rosenfeld et al.,  
56 2008; Yang et al., 2022a). Due to the absorption of solar radiation, aerosol-induced heating can  
57 strengthen temperature inversion and increase the atmospheric stability, which inhibits the  
58 vertical mixing and transport of aerosols and leads to a further increase in near-surface aerosol  
59 concentrations (Chen et al., 2021; Lou et al., 2019). Therefore, knowing the sources of aerosols  
60 and their variations have become a vital direction in the field of environmental and atmospheric  
61 sciences.

62 Human activities have a great influence on global aerosol distributions and compositions.  
63 For example, many countries have taken various air quality control measures at different stages  
64 of their economic development, causing distinct historical temporal changes of aerosol  
65 emissions across the world. Since the start of industrialization, anthropogenic emissions of  
66 aerosols and precursor gases have substantially increased, which significantly affected the  
67 atmospheric environment and the Earth's energy balance (Carslaw et al., 2013). European and  
68 North American countries became major contributors of pollutant emissions. Since the 1980s,  
69 coal emissions have declined steadily in Europe and North America owing to the legislation

70 and effective environmental policies to reduce local anthropogenic emissions of aerosol and  
71 precursor gases (Smith et al., 2011). In contrast to North America and Europe, the coal  
72 consumption in China and India has experienced a substantial increase and anthropogenic  
73 emissions from these regions continued to rise (Hoesly et al., 2018; Lim et al., 2020). Zheng et  
74 al. (2018) also reported that due to active clean air policies and the emission control of power  
75 plants and industry, anthropogenic emissions of PM<sub>2.5</sub> (particulate matter less than 2.5 µm in  
76 diameter) from China have significantly decreased by 33% during 2013–2017. However,  
77 countries in South Asia still rely on coal and petroleum and thus aerosol emissions from South  
78 Asia have kept increasing in recent years (Li et al., 2017).

79 Regional aerosol pollution can be induced by both local emissions and long-range  
80 transport of pollutants across regions, countries or even continents, which impose a far-  
81 reaching impact on air quality and human health (Akimoto, 2003; Anenberg et al., 2014; Jaffe  
82 et al., 1999; Lin et al., 2014; Liu et al., 2009; Zhang et al., 2017). Studies reported that the air  
83 quality in Europe is largely impacted by the long-range aerosol transport from North America  
84 (Stohl and Trickl, 1999; Yang et al., 2018a, 2020b). Asian anthropogenic emissions in spring  
85 also have a significant effect on the aerosol concentrations in North America (Jaffe et al.,  
86 1999). Moreover, studies found that air pollution from Africa and Europe moved eastward and  
87 merged with Asian pollution, affecting air quality in western North America (Liu et al., 2005;  
88 Chin et al., 2007). Yang et al. (2017) also found that remote sources contributed the most to  
89 the regions with low emissions through long-range transport, which further impacted the local  
90 climate. Therefore, relying on the domestic emission control alone may be insufficient to  
91 prevent air pollution due to the long-distance transport of air pollutants (Liu et al., 2009). A

92 study revealed that approximately 12% of global premature deaths caused by PM<sub>2.5</sub> were  
93 related to non-local air pollutants (Zhang et al., 2017). About 16% of premature deaths in India  
94 caused by PM<sub>2.5</sub> were attributed to aerosol transport from external source regions (David et al.,  
95 2019). Within each emission source region, aerosols also come from different emission sectors.  
96 Many scientific control measures and policies are implemented based on the source attribution  
97 of air pollutants from individual sectors. Hence, it is of great significance to quantify source  
98 contributions of long-range transport of aerosols from major emission regions of the world as  
99 well as aerosols from major emission sectors.

100 Anthropogenic emissions of aerosols and precursor gases have changed significantly in  
101 different source regions over the past century. Few studies focus on the source attributions of  
102 aerosols across the globe over such a long period of time. In this study, we focus on the changes  
103 in aerosols and emission source region and sector contributions in major source regions (i.e.,  
104 North America, Europe, East Asia, South Asia) during the three important periods of emission  
105 changes since industrialization (1850–1980, 1980–2010 and 2010–2017) based on the  
106 Energy Exascale Earth System Model version 1 (E3SMv1), equipped with an explicit aerosol  
107 source tagging system (E3SMv1-EAST).

## 108 **2. Methods**

### 109 **2.1. Model description and experimental design**

110 To study variations in historical anthropogenic aerosols in the major source regions, the  
111 E3SMv1 developed by US Department of Energy (DOE) (Golaz et al., 2019) is used in this  
112 study. The E3SMv1 model is updated on the basis of Community Atmosphere Model version  
113 5 (CAM5) in order to explore several key emerging issues in the field of environment and

114 climate, and is a branch of the widely-used Community Earth System Model (CESM) (Rasch  
115 et al., 2019). E3SMv1 consists of atmosphere, land surface, ocean, sea ice, and river model  
116 components. It features numerous upgrades to aerosol, turbulence, chemical, and cloud-related  
117 processes, offering multiple spatial resolution options. The model can run simulations for  
118 decades or more at higher resolution to help understand past, present, and future changes in  
119 Earth's behavior, and to explore how the atmosphere interacts with other components of the  
120 Earth system. Aerosol microphysics and interactions with stratiform clouds are treated with the  
121 four-mode Modal Aerosols Module (MAM4) (Liu et al., 2016), which predicts the mass and  
122 number concentrations of sulfate, black carbon (BC), primary organic matter (POM),  
123 secondary organic aerosol (SOA), marine organic aerosol, mineral dust and sea salt (Wang et  
124 al., 2020). EAMv1 applies the “Morrison and Gettelman version 2” (MG2) two-moment bulk  
125 microphysics parameterization for stratiform clouds (Gettelman and Morrison, 2015). It allows  
126 aerosol-cloud interactions in all stratiform and shallow convective clouds but neglects in deep  
127 convective clouds (Rasch et al., 2019). Liquid cloud drop activation is based on Abdul-Razzak  
128 and Ghan (2000) and a classical nucleation theory-based ice nucleation parameterization for  
129 the heterogeneous ice formation in mixed-phase clouds follows Y. Wang et al. (2014).  
130 Hygroscopicity are specified for soluble aerosols to calculate the particle size based on relative  
131 humidity. The aerosols are assumed to mix internally in the same aerosol mode and externally  
132 between modes when calculating the aerosol optical properties (Ghan and Zaveri, 2007). The  
133 model has been applied to investigate the variations in anthropogenic and natural aerosols  
134 related to the air-sea interactions (Yang et al., 2022b; Zeng et al., 2021). Compared to the  
135 regional model, the E3SMv1 with an aerosol tagging tool introduced in this study is more

136 suitable for the simulation of transboundary and intercontinental transport of aerosols across  
137 the globe. In this study, the model is configured at its standard horizontal spatial resolution of  
138 approximately  $1^\circ$  with 72 vertical layers.

139 Global emissions of aerosols and precursor gases used in the simulations are obtained  
140 from the CMIP6 (the Coupled Model Intercomparison Project Phase 6) datasets (Hoesly et al.,  
141 2018; van Marle et al., 2017). However, the anthropogenic emissions in China are replaced  
142 with MEIC (Multi-resolution Emission Inventory for China) inventory, which fully considers  
143 the implementation of clean air actions over China since the 2010s (Gao et al., 2022, 2023; Li  
144 et al., 2021; Zheng et al., 2018). Following previous studies (Ren et al., 2021; Yang et al.,  
145 2018a), the near-surface concentrations of  $PM_{2.5}$  here are estimated as the sum of sulfate, BC,  
146 POM and SOA concentrations. Effective radiative forcing (ERF) refers to the change of the  
147 net radiative flux at the top of the atmosphere (TOA) after the external forcing is applied. In  
148 this study, ERF due to aerosol-radiation interactions ( $ERF_{ari}$ ) for the individual tagged source  
149 regions is derived as the difference in TOA net radiative fluxes from a pair of diagnostic  
150 radiation calculations with and without the particular tagged aerosols from the source regions  
151 for the all-sky condition following Ghan (2013).

152 This study focuses on the variations in source region and sector contributions in four major  
153 emission regions of the world (North America, Europe, East Asia and South Asia) during the  
154 three key historical periods of emission changes (1850–1980, 1980–2010 and 2010–2017).  
155 Four simulations with monthly anthropogenic emissions of aerosols and precursors fixed at the  
156 1850, 1980, 2010 and 2017 levels, respectively, are conducted. All simulations are performed  
157 for one year following 6-month model spin-up. Greenhouse gas concentrations, solar insolation,



158 sea surface temperature and sea ice extent are prescribed at the 2000 levels. The meteorological  
159 fields including 3-dimensional temperature, specific humidity, and winds are nudged toward  
160 the MERRA-2 (Modern-Era Retrospective Analysis for Research and Applications, version 2)  
161 reanalysis (Gelaro et al., 2017) in year 2017 at a 6-hourly relaxation timescale.

## 162 **2.2. Explicit aerosol source tagging system**

163 Source apportionment aims to quantify the contributions to aerosols from specific sources.  
164 To examine the source-receptor relationships of aerosols, we implemented the Explicit Aerosol  
165 Source Tagging (EAST) in E3SMv1, which play a critical role in attributing aerosol  
166 concentrations to their respective emission sources. The EAST follows the BC source-tagging  
167 technique introduced in H. Wang et al. (2014), sulfate source-tagging method used in Yang et  
168 al. (2017) and other carbonaceous aerosol-tagging applied in Yang et al. (2018a), which was  
169 previously implemented in the Community Atmosphere Model version 5 (CAM5-EAST). This  
170 tagging system is different from the traditional emission sensitivity method that zero out or  
171 perturb emissions from a given source region or sector in sensitivity simulations along with a  
172 baseline simulation, which has to assume a linear response to emission perturbation and  
173 requires many additional simulations for estimating the contributions from multiple sources  
174 (Wang et al., 2014). EAST independently considers all aerosol physical, chemical, and  
175 dynamical processes for each tagged sources through introducing additional aerosol-related  
176 variables within one simulation and it does not rely on a linear response to emission  
177 perturbations. These capabilities make it physically more accurate and time saving than the  
178 sensitivity experiments. This tagging method has previously been adopted in regional models

179 and has now implemented in the global E3SMv1 model to better understand the  
180 intercontinental transport from sources outside the regional domain.

181 In this study, totally 18 tags are set for each anthropogenic species of aerosols and  
182 precursors. Each of the 4 major source regions, including North America (NAM), Europe  
183 (EUR), East Asia (EAS) and South Asia (SAS), has 4 tags for the energy transformation and  
184 extraction (ENE), industrial combustion and processes (IND), residential, commercial and  
185 other (RCO) and the rest of anthropogenic emission sectors (RST). One tag is assigned to the  
186 anthropogenic emissions from rest of the world (ROW) and the last tag is allocated for all the  
187 natural/biogenic sources including open biomass burning, volcanic emissions and oceanic  
188 emissions.

### 189 **2.3. Model evaluation**

190 In order to evaluate the performance of E3SMv1 in reproducing the aerosol concentrations,  
191 Fig. 2 compares the simulated near-surface PM<sub>2.5</sub> concentrations with the observations from  
192 the Interagency Monitoring of Protected Visual Environments (IMPROVE) over the U.S., the  
193 European Monitoring and Evaluation Programme (EMEP) over Europe, the U.S. embassies  
194 and consulates in India and the China National Environmental Monitoring Center (CNEMC)  
195 over China in year 2017. The model successfully reproduces the spatial distribution of PM<sub>2.5</sub>  
196 concentrations, with relatively high concentrations in eastern China, India and low  
197 concentrations in the U.S. and Europe. The spatial correlation coefficient (R) between the  
198 E3SMv1 simulated PM<sub>2.5</sub> concentrations and observations is +0.80. The model well reproduces  
199 the PM<sub>2.5</sub> concentrations in the U.S. with the normalized mean biases (NMB) of -11%.  
200 However, it largely underestimates the PM<sub>2.5</sub> concentrations in China and Europe, which has

201 also been revealed in several studies (e.g., Gao et al., 2018; Gao et al., 2023; Navinya et al.,  
202 2020; Zeng et al., 2021). This discrepancy is partly because E3SMv1 only considers limited  
203 aerosol species (BC, POM, SOA and sulfate) without including nitrate and ammonium aerosols  
204 in the aerosol module. On the other hand, the overestimated wet scavenging at the mid- and  
205 high latitudes and underestimated gas-to-particle conversion can also lead to the low bias (Zeng  
206 et al., 2021). The evaluation in 2010 also shows similar high correlation and biases (Fig. S3).

207 In order to evaluate the model performance in reproducing the historical changes in  
208 aerosol concentrations during the important periods of emission changes, the variations in near-  
209 surface PM<sub>2.5</sub> concentrations are compared with observations (Fig. S4) and MERRA-2  
210 reanalysis (Fig. S5). The model well reproduces the decreases in PM<sub>2.5</sub> concentrations in the  
211 eastern U.S. and Europe and the increases in East Asia and South Asia during 1980–2010, with  
212 the spatial R of 0.78 between model results and MERRA-2 data. The model also well simulates  
213 the aerosol decline in North America, Europe, and East Asia and a continuous increase in South  
214 Asia during 2010–2017, with the R of 0.81 between model results and observational data.  
215 However, the model simulation does capture the increases in PM<sub>2.5</sub> in southwestern Canada  
216 and eastern Russia. It is because the wildfire emissions were kept unchanged during the  
217 simulation, while wildfires occurred more frequently in these regions during the analyzed time  
218 period (Jolly et al., 2015; Goss et al., 2020), leading to the increases in PM<sub>2.5</sub> in observations.

### 219 **3. Results**

#### 220 **3.1. Historical changes in aerosols over major source regions**

221 Figure 3 shows the variations in anthropogenic emissions of sulfur dioxide (SO<sub>2</sub>) during  
222 the three key periods of historical emission changes from the tagged source regions. Since

223 industrialization, anthropogenic SO<sub>2</sub> emissions had rising trends during 1850–1980, especially  
224 in Europe and North America. Due to the implementation of clean air actions in western  
225 countries, SO<sub>2</sub> emissions in North America and Europe declined considerably during 1980–  
226 2010, while the emissions in East Asia and South Asia continued to increase. After 2010, China  
227 issued several clean air policies, which led to significant decreases in anthropogenic SO<sub>2</sub>  
228 emissions in East Asia, while the SO<sub>2</sub> emissions in South Asia kept increasing during 2010–  
229 2017. The changes in anthropogenic BC and organic carbon (OC) emissions are similar to those  
230 of SO<sub>2</sub> (shown in Figure S1 and S2).

231       The changes in near-surface mass concentrations (Fig. 4) and column burdens (Fig. 5) of  
232 anthropogenic PM<sub>2.5</sub> contributed by the tagged source regions during the focused three  
233 historical time periods follow the corresponding changes in anthropogenic emissions. Column  
234 burden refers to the concentration of aerosols contained in the air column above a unit area  
235 with a top at 60 km, which can better reflect the aerosol transport within the air column and is  
236 more related to the aerosol radiative effect. The near-surface concentration of aerosols  
237 represents the concentration of aerosols in the air near the surface (from the surface to 997 hPa  
238 for model layer), which is more related to air quality and human health. Local anthropogenic  
239 emission changes drove the PM<sub>2.5</sub> to reach its peak in 1980 in North America and Europe and  
240 then to decrease. The maximum PM<sub>2.5</sub> appeared in 2010 in East Asia and the anthropogenic  
241 PM<sub>2.5</sub> level continued growing in South Asia during 1850–2017, consistent with previous  
242 studies (Dey et al.,2020; Guttikunda et al., 2022; Singh et al.,2023).

243       To explore which aerosol species contributed the most to the changes in PM<sub>2.5</sub> during the  
244 focused three historical time periods, Figs. 6 and 7 illustrate the relative contributions of

245 individual aerosols to the simulated changes in near-surface  $PM_{2.5}$  mass concentrations and  
246 column burdens, respectively, in four major emission regions. In general, the historical changes  
247 in anthropogenic  $PM_{2.5}$  were primarily driven by the changes in sulfate. In North America, the  
248 contribution of sulfate to near-surface  $PM_{2.5}$  concentration (column burden) rose from 7%  
249 (11%) in 1850 to 67% (81%) in 1980, then dropped to 52% (67%) in 2017. In Europe, sulfate  
250 contribution changed from 24% (34%) in 1850 to 71% (85%) in 1980, then decreased to 50%  
251 (68%) in 2017. In East Asia, sulfate contribution changes from 2% (6%) in 1850 to 51% (71%)  
252 in 1980, then decreased to 33% (56%) in 2017. It is interesting that the  $PM_{2.5}$  levels in East  
253 Asia increased during 1980–2010, but the sulfate contribution decreased in this time period. It  
254 is because the carbonaceous aerosols increased remarkably, which reduced the fractional  
255 contribution of sulfate. The sulfate contribution to  $PM_{2.5}$  concentration (column burden)  
256 increased throughout the period of 1850–2017, from 2% (5%) to 42% (62%) in South Asia.  
257 Note that the carbonaceous aerosols, especially POM, dominated the  $PM_{2.5}$  in all four targeted  
258 regions in 1850, resulting from the high heating demand from the residential sector.

### 259 **3.2 Changes in contributions from major source regions and sectors**

260 Figure 8 shows the relative contributions from local and remote anthropogenic sources to  
261 the near-surface concentrations and column burdens of  $PM_{2.5}$  in the four targeted regions in  
262 2010. Local sources dominated the near-surface anthropogenic  $PM_{2.5}$  concentrations over the  
263 high emission regions including eastern China, eastern U.S. and Indo-Gangetic Plain, with  
264 local contributions being higher than 90%. In the regions with low emissions, such as the  
265 Tibetan Plateau, the anthropogenic  $PM_{2.5}$  concentrations were largely contributed by the long-  
266 range transport of aerosols. The spatial distributions of burden contribution are similar to those

267 of corresponding contribution near the surface, but the long-range transport contributed more  
268 to the column burden than to the near-surface contribution due to the more efficient pollutant  
269 transport in the free troposphere than within the boundary layer. The long-range transport  
270 contributes 30%–35% of PM<sub>2.5</sub> burden in East Asia and South Asia and 50–55% in North  
271 America and Europe, much higher than the 10%–25% for the near-surface concentrations over  
272 the four targeted regions.

273 Since both local and remote emissions can contribute to the anthropogenic PM<sub>2.5</sub>, it is  
274 valuable to know the historical changes in these contributions, especially by the local sources  
275 from individual emission sectors and by remote sources from major emission regions. Figure  
276 9 illustrates changes in the local source contributions from major emission sectors to the near-  
277 surface concentrations and column burdens of PM<sub>2.5</sub> during 1850–2017. In North America and  
278 Europe, the historical changes in anthropogenic PM<sub>2.5</sub> were largely induced by changes in  
279 emissions from the local energy (ENE) sector, followed by the industry (IND) sector, which  
280 increased before 1980 and decreased afterward. In East Asia, ENE, IND and residential (RCO)  
281 sector emissions all had significant contributions to the increases in PM<sub>2.5</sub> concentration and  
282 burden from 1850 to 1980. Then the contribution from local IND sector showed the largest  
283 increases from 1980 to 2010 and decreases from 2010 to 2017. In South Asia, the  
284 anthropogenic PM<sub>2.5</sub> increases from 1850 to 1980 were mainly attributed to the RCO emission  
285 increases. After that, increases in ENE emissions dominated the rising PM<sub>2.5</sub> levels in South  
286 Asia during 1980–2017.

287 Figure 10 presents changes in remote emission contributions from the tagged source  
288 regions to the column burdens of PM<sub>2.5</sub> during 1850–2017. The contributions from long-range

289 transport to the near-surface concentrations and their historical variations over the four major  
290 emissions regions are relatively small, which were also reported in previous studies (e.g., Yang  
291 et al., 2018b) and are not discussed here. During 1850–1980, the long-range transport  
292 contributions to the PM<sub>2.5</sub> burdens show increases and the contributions from ROW increased  
293 the most among the tagged source regions over all four targeted receptor regions. Note that  
294 aerosol emissions from North America contributed to the increase in European PM<sub>2.5</sub> burden  
295 by 1.7 mg m<sup>-2</sup> and sources from Europe were also responsible for the PM<sub>2.5</sub> burden increase by  
296 1.0 mg m<sup>-2</sup> in East Asia and 1.1 mg m<sup>-2</sup> in South Asia. During 1980–2010, the long-range  
297 transport from North America and Europe decreased, but that from East Asia and South Asia  
298 increased. East Asia contributed 0.4–0.6 mg m<sup>-2</sup> to the PM<sub>2.5</sub> burden increases in North  
299 America, while Europe and South Asia contributed about 0.3 mg m<sup>-2</sup>. In East Asia, 1.6 mg m<sup>-2</sup>  
300 of the PM<sub>2.5</sub> burden increase was attributed to South Asian sources and 0.8 mg m<sup>-2</sup> of the  
301 PM<sub>2.5</sub> burden increase in South Asia during this time period was due to increases in East Asian  
302 emissions. From 2010 to 2017, owing to the clean air actions in China, contributions from East  
303 Asia to the PM<sub>2.5</sub> burdens in the other three targeted regions decreased by 0.3–0.6 mg m<sup>-2</sup>.  
304 However, due to the continuous increases in South Asian emissions, South Asia still  
305 contributed to the PM<sub>2.5</sub> burden increase in East Asia by 0.4 mg m<sup>-2</sup> during this short time  
306 period.

### 307 **3.3 Changes in effective radiative forcing due to aerosol-radiation interactions**

308 The variation in aerosols can have a significant impact on ERF through aerosol-radiation  
309 and aerosol-cloud interactions. Figure 11 shows changes in ERF due to aerosol-radiation  
310 interactions (ERF<sub>ari</sub>) at the top of the atmosphere (TOA) that can be attributed to changes in

311 anthropogenic emissions from the tagged regions in the three key periods during 1850–2017.  
312 Due to the increases in aerosols from 1850 to 1980, a large negative  $ERF_{ari}$  was located over  
313 the major source regions and their downwind areas, with maximum  $ERF_{ari}$  changes being larger  
314 than  $2 \text{ W m}^{-2}$  over eastern U.S., Europe and eastern China. In 2010, there were positive  $ERF_{ari}$   
315 changes (warming effect) by a maximum of  $2 \text{ W m}^{-2}$  in North America and Europe compared  
316 to 1980, which were due to the decreases in anthropogenic aerosols in these two regions. The  
317 positive  $ERF_{ari}$  changes due to the decrease in North American aerosols extended across the  
318 North Atlantic and caused an increase in incoming radiation by up to  $0.5 \text{ W m}^{-2}$  in Europe.  
319 Similarly, the decrease in aerosols from Europe also led to a positive  $ERF_{ari}$  change by up to  
320  $0.5 \text{ W m}^{-2}$  in the downwind regions including Russia and northern China during 1980–2010.  
321 This is also revealed by previous studies that aerosol reduction has caused fast warming in  
322 downwind regions (Urdiales-Flores et al., 2023). Increases in aerosols in China during 1980–  
323 2010 and decreases during 2010–2017 produced negative (cooling) and positive (warming)  
324 changes in  $ERF_{ari}$ , respectively, over eastern China and North Pacific, which largely  
325 contradicted each other. The continuously growing aerosols in South Asia induced negative  
326  $ERF_{ari}$  changes (cooling) in South Asia, Southeast Asia and southern China during both 1980–  
327 2010 and 2010–2017. Note that in this study we only quantify the  $ERF_{ari}$  for the major emission  
328 regions based on the source tagging technique. The quantification of ERF due to aerosol-cloud  
329 interactions ( $ERF_{aci}$ ) requires additional simulations, which could be further examined in future  
330 studies.

#### 331 **4. Conclusions and Discussions**



332 Since the start of industrialization, aerosols have changed significantly in different regions  
333 of the world driven by global economic development and air pollution control measures. It is  
334 of great significance to quantify the contributions of aerosols from major emission source  
335 regions and sectors during the key periods of substantial emission changes. In this study, the  
336 Explicit Aerosol Source Tagging (EAST) technique is implemented in E3SMv1 to quantify the  
337 variations in the concentrations, source contributions, and the subsequent effective radiative  
338 forcing of anthropogenic aerosols in four major source regions (NAM, EUR, EAS and SAS)  
339 during three key historical periods of emission changes (1850–1980, 1980–2010 and 2010–  
340 2017).

341 Following the corresponding anthropogenic emission changes,  $PM_{2.5}$  concentrations  
342 reached its peak in 1980 in North America and Europe, while the peak of  $PM_{2.5}$  in East Asia  
343 occurred in 2010. The  $PM_{2.5}$  from anthropogenic sources in South Asia continued growing  
344 during 1850–2017. These changes in anthropogenic  $PM_{2.5}$  were primarily dominated by  
345 changes in sulfate aerosol. In North America and Europe, historical changes in anthropogenic  
346  $PM_{2.5}$  were mainly caused by changes in emissions from local energy sector, followed by the  
347 industrial sector, which increased from 1850 to 1980 and decreased afterward. In East Asia,  
348 energy, industrial, and residential emissions contributed significantly to the increase in  $PM_{2.5}$   
349 from 1850 to 1980, then the local industrial sector caused the most increase from 1980 to 2010,  
350 and declined from 2010 to 2017. For South Asia, the increase in  $PM_{2.5}$  was mainly due to  
351 emission changes in the residential sector from 1850 to 1980, then the increase in energy-  
352 related emissions became dominant to the rise of  $PM_{2.5}$  levels during 1980–2017.

353 Regional aerosol pollution comes from both local emissions and long-range transport of  
354 remote emissions. Local emissions contribute the most in regions with high emissions, while  
355 in regions with low emissions the long-distance transport plays an important role. Due to the  
356 more efficient transport of air pollutants in the free troposphere, contributions of long-range  
357 transport to column burden are greater than to the near-surface concentration over all four  
358 targeted receptor regions. From 1850 to 1980, increases in emissions from North America  
359 contributed to the increase in European  $\text{PM}_{2.5}$  burden by  $1.7 \text{ mg m}^{-2}$  and emissions from Europe  
360 were also responsible for the  $\text{PM}_{2.5}$  burden increase by  $1.0 \text{ mg m}^{-2}$  in East Asia and  $1.1 \text{ mg m}^{-2}$   
361 in South Asia. From 1980 to 2010, the long-range transport from North America and Europe  
362 decreased, while those from East Asia and South Asia increased. East Asia contributed  $0.4\text{--}$   
363  $0.6 \text{ mg m}^{-2}$  to the  $\text{PM}_{2.5}$  burden increases in North America, while Europe and South Asia  
364 contributed about  $0.3 \text{ mg m}^{-2}$ . In East Asia,  $1.6 \text{ mg m}^{-2}$  of the  $\text{PM}_{2.5}$  burden increase was  
365 attributed to South Asian sources and  $0.8 \text{ mg m}^{-2}$  of the  $\text{PM}_{2.5}$  burden increase in South Asia  
366 during this time period was due to the increases in East Asian emissions. From 2010 to 2017,  
367 the contributions from East Asia to the  $\text{PM}_{2.5}$  burdens in the other three targeted regions  
368 declined by  $0.3\text{--}0.6 \text{ mg m}^{-2}$  due to Clean Air actions in China. However, due to the continuous  
369 increase of emissions in South Asia, the  $\text{PM}_{2.5}$  burden in East Asia still increased by  $0.4 \text{ mg m}^{-2}$ .  
370

371 Changes in aerosols can have a significant impact on ERF, which further imposes an  
372 impact on climate. Large negative  $\text{ERF}_{\text{ari}}$  appeared over the major source regions and their  
373 downwind areas during 1850–1980 due to the increases in aerosol emissions, with maximum  
374  $\text{ERF}_{\text{ari}}$  changes being larger than  $2 \text{ W m}^{-2}$  over eastern North America, Europe and eastern

375 China. From 1980 to 2010, a positive  $ERF_{ari}$  change caused by a decline in North American  
376 aerosols extended over the North Atlantic, resulting in a warming of up to  $0.5 \text{ W m}^{-2}$  in Europe.  
377 Meanwhile, a decline of aerosols in Europe also caused a warming of up to  $0.5 \text{ W m}^{-2}$  in Russia  
378 and northern China. The changes in  $ERF_{ari}$  from the increase (from 1980 to 2010) and decrease  
379 (from 2010 to 2017) of aerosols in China had an opposite sign. The continuous aerosol  
380 increases in South Asia from 1980 to 2017 resulted in negative  $ERF_{ari}$  changes in South Asia,  
381 Southeast Asia, and southern China.

382 This study provides an in-depth analysis of historical changes in anthropogenic aerosol  
383 concentrations, compositions, source contributions and radiative impacts in the four major  
384 emission source regions of the globe, which has important implications for the pollution  
385 prevention/control measures and decision making for global collaboration. The spatial  
386 distribution and changes in anthropogenic aerosols are similar to those reported in previous  
387 studies (Hoesly, et al., 2018; Lim, et al., 2020). However, we also note that the E3SMv1 model  
388 underestimates the near-surface  $PM_{2.5}$  concentrations in Europe and East Asia, which could  
389 lead to an underestimate of the corresponding radiative and climate impact. Our analysis  
390 focuses on aerosols from anthropogenic emissions; however, with the increasing attention to  
391 air quality in many countries around the world, anthropogenic aerosol concentrations are  
392 declining and contributions from biomass burning aerosols are becoming more and more  
393 important. The source contributions and impacts of biomass burning aerosols will be  
394 investigated in our future work. Also, this study only quantifies the  $ERF_{ari}$  for individual major  
395 emission regions based on the source tagging technique and radiation diagnostic calculations.

396 The quantification of  $ERF_{aci}$  requires additional simulations, which could be further examined  
397 in future studies.

398 **Author contributions.** YY designed the research, added the tagging code and performed  
399 simulations; SM analyzed the data. All authors including HW, PW, and HL discussed the  
400 results and wrote the paper.

401

402 **Code and data availability.** The E3SMv1 model is available at <https://github.com/E3SM->  
403 [Project/E3SM](https://github.com/E3SM-Project/E3SM)(last access:1 October 2022) (<https://doi.org/10.11578/E3SM/dc.20180418.36>;  
404 E3SM Project, 2018). Our results can be made available upon request.

405

406 **Acknowledgments.** HW acknowledges the support by the U.S. Department of Energy (DOE),  
407 Office of Science, Office of Biological and Environmental Research (BER), as part of the  
408 Earth and Environmental System Modeling program. The Pacific Northwest National  
409 Laboratory (PNNL) is operated for DOE by the Battelle Memorial Institute under contract  
410 DE-AC05-76RLO1830.

411

412 **Financial support.** This study was supported by the National Key Research and  
413 Development Program of China (grant 2020YFA0607803 and 2019YFA0606800), the  
414 National Natural Science Foundation of China (grant 41975159), Jiangsu Science Fund for  
415 Distinguished Young Scholars (grant BK20211541), and the Jiangsu Science Fund for  
416 Carbon Neutrality (grant no. BK20220031).

417

418 **Conflict of interest.**

419 At least one of the (co-)authors is a member of the editorial board of ACP.

420 **References**

- 421
- 422 Abdul-Razzak, H. and Ghan, S. J.: A parameterization of aerosol activation, 2. Multiple  
423 aerosol types, *J. Geophys. Res.*, 105, 6837–6844,  
424 <https://doi.org/10.1029/1999JD901161>, 2000.
- 425
- 426 Akimoto, H.: Global Air Quality and Pollution, *Science*, 302, 1716–1719,  
427 <https://doi.org/10.1126/science.1092666>, 2003.
- 428
- 429 Anenberg, S. C., Horowitz, L. W., Tong, D. Q., and West, J. J.: An Estimate of the Global  
430 Burden of Anthropogenic Ozone and Fine Particulate Matter on Premature Human  
431 Mortality Using Atmospheric Modeling, *Environ. Health Perspect.*, 118, 1189–1195,  
432 <https://doi.org/10.1289/ehp.0901220>, 2010.
- 433
- 434 Anenberg, S. C., West, J. J., Yu, H., Chin, M., Schulz, M., Bergmann, D., Bey, I., Bian, H.,  
435 Diehl, T., Fiore, A., Hess, P., Marnmer, E., Montanaro, V., Park, R., Shindell, D.,  
436 Takemura, T., and Dentener, F.: Impacts of intercontinental transport of anthropogenic  
437 fine particulate matter on human mortality, *Air. Qual. Atmos. Health.*, 7, 369–379,  
438 <https://doi.org/10.1007/s11869-014-0248-9>, 2014.
- 439
- 440 Carslaw, K. S., Gordon, H., Hamilton, D. S., Johnson, J. S., Regayre, L. A., Yoshioka, M.,  
441 and Pringle, K. J.: Aerosols in the Pre-industrial Atmosphere, *Curr. Clim. Change Rep.*,  
442 3, 1–15, <https://doi.org/10.1007/s40641-017-0061-2>, 2017.
- 443
- 444 Chen, D., Liao, H., Yang, Y., Chen, L., and Wang, H.: Simulated aging processes of black  
445 carbon and its impact during a severe winter haze event in the Beijing-Tianjin-Hebei  
446 region, *Sci. Total Environ.*, 755, 142712,  
447 <https://doi.org/10.1016/j.scitotenv.2020.142712>, 2021.
- 448
- 449 Chin, M., Diehl, T., Ginoux, P., and Malm, W.: Intercontinental transport of pollution and  
450 dust aerosols: implications for regional air quality, *Atmos. Chem. Phys.*, 7, 5501–5517,  
451 <https://doi.org/10.5194/acp-7-5501-2007>, 2007.
- 452
- 453 David, L. M., Ravishankara, A. R., Kodros, J. K., Pierce, J. R., Venkataraman, C., and  
454 Sadavarte, P.: Premature mortality due to PM<sub>2.5</sub> over India: Effect of atmospheric  
455 transport and anthropogenic emissions, *Geohealth*, 3, 2–10,  
456 <https://doi.org/10.1029/2018GH000169>, 2019.
- 457
- 458 Dey, S., Purohit, B., Balyan, P., Dixit, K., Bali, K., Kumar, A., Imam, F., Chowdhury, S.,  
459 Ganguly, D., Gargava, P., and Shukla, V. K.: A satellite-based high-resolution (1-km)  
460 ambient PM<sub>2.5</sub> database for India over two decades (2000–2019): applications for air  
461 quality management, *Remote Sens.*, 12, 3872, <https://doi.org/10.3390/rs12233872>, 2022.
- 462

463 Finlayson-Pitts, B. J., and Pitts, J. N.: Tropospheric Air Pollution: Ozone, Airborne Toxics,  
464 Polycyclic Aromatic Hydrocarbons, and Particles, *Science*, 276, 1045–1051,  
465 <https://doi.org/10.1126/science.276.5315.1045>, 1997.  
466

467 Gao, M., Beig, G., Song, S., Zhang, H., Hu, J., Ying, Q., Liang, F., Liu, Y., Wang, H., Lu, X.,  
468 Zhu, T., Carmichael, G. R., Nielsen, C. P., McElroy, M. B.: The impact of power  
469 generation emissions on ambient PM<sub>2.5</sub> pollution and human health in China and India,  
470 *Environ. Int.*, 121, 250-259, <https://doi.org/10.1016/j.envint.2018.09.015>, 2018.  
471

472 Gao, J., Yang, Y., Wang, H., Wang, P., Li, H., Li, M., Ren, L., Yue, X., and Liao, H.: Fast  
473 climate responses to emission reductions in aerosol and ozone precursors in China  
474 during 2013–2017, *Atmos. Chem. Phys.*, 22, 7131–7142, <https://doi.org/10.5194/acp-22-7131-2022>, 2022.  
475

476

477 Gao, J., Yang, Y., Wang, H., Wang, P., Li, B., Li, J., Wei, J., Gao, M., and Liao, H.: Climate  
478 responses in China to domestic and foreign aerosol changes due to clean air actions  
479 during 2013–2019, *npj Clim. Atmos. Sci.*, 6, 160, <https://doi.org/10.1038/s41612-023-00488-y>, 2023.  
480

481

482 Gelaro, R., McCarty, W., Suárez, M. J., Todling, R., Molod, A., Takacs, L., Randles, C. A.,  
483 Darmenov, A., Bosilovich, M. G., Reichle, R., Wargan, K., Coy, L., Cullather, R.,  
484 Draper, C., Akella, S., Buchard, V., Conaty, A., da Silva, A. M., Gu, W., Kim, G.,  
485 Koster, R., Lucchesi, R., Merkova, D., Nielsen, J. E., Partyka, G., Pawson, S., Putman,  
486 W., Rienecker, M., Schubert, S. D., Sienkiewicz, M., and Zhao, B.: The Modern-Era  
487 Retrospective Analysis for Research and Applications, Version 2 (MERRA-2), *J.*  
488 *Climate*, 30, 5419–5454, <https://doi.org/10.1175/JCLI-D-16-0758.1>, 2017.  
489

490 Ghan, S. J.: Technical Note: Estimating aerosol effects on cloud radiative forcing, *Atmos.*  
491 *Chem. Phys.*, 13, 9971–9974, <https://doi.org/10.5194/acp-13-9971-2013>, 2013.  
492

493 Ghan, S. J. and Zaveri, R. A.: Parameterization of optical properties for hydrated internally  
494 mixed aerosol, *J. Geophys. Res.-Atmos.*, 112, D10201,  
495 <https://doi.org/10.1029/2006JD007927>, 2007.  
496

497 Golaz, J. C., Caldwell, P. M., Van Roekel, L. P., Petersen, M. R., Tang, Q., Wolfe, J. D.,  
498 Abeshu, G., Anantharaj, V., Asay-Davis, X. S., Bader, D. C., Baldwin, S. A., Bisht, G.,  
499 Bogenschutz, P. A., Branstetter, M., Brunke, M. A., Brus, S. R., Burrows, S. M.,  
500 Cameron-Smith, P. J., Donahue, A. S., Deakin, M., Easter, R. C., Evans, K. J., Feng, Y.,  
501 Flanner, M., Foucar, J. G., Fyke, J. G., Griffin, B. M., Hannay, C., Harrop, B. E.,  
502 Hoffman, M. J., Hunke, E. C., Jacob, R. L., Jacobsen, D. W., Jeffery, N., Jones, P. W.,  
503 Keen, N. D., Klein, S. A., Larson, V. E., Leung, L. R., Li, H. Y., Lin, W., Lipscomb, W.  
504 H., Ma, P., Mahajan, S., Maltrud, M. E., Mامتjanov, A., McClean, J. L., McCoy, R.  
505 B., Neale, R. B., Price, S. F., Qian, Y., Rasch, P. J., Eyre, J. E. J. R., Riley, W. J.,  
506 Ringler, T. D., Roberts, A. F., Roesler, E. L., Salinger, A. G., Shaheen, Z., Shi, X.,

507 Singh, B., Tang, J., Taylor, M. A., Thornton, P. E., Turner, A. K., Veneziani, M., Wan,  
508 H., Wang, H., Wang, S., Williams, D. N., Wolfram, P. J., Worley, P. H., Xie, S., Yang  
509 Y., Yoon, J., Zelinka, M. D., Zender, C. S., Zeng, X., Zhang, C., Zhang, K., Zhang, Y.,  
510 Zheng, X., Zhou, T., and Zhu, Q.: The DOE E3SM Coupled Model Version 1:  
511 Overview and Evaluation at Standard Resolution, *J. Adv. Model. Earth Syst.*, 11, 2089–  
512 2129. <https://doi.org/10.1029/2018MS001603>, 2019.

513

514 Goss, M., Swain, D. L., Abatzoglou, J. T., Sarhadi, A., Kolden, C. A., Williams A. P., and  
515 Diffenbaugh, N. S.: Climate change is increasing the likelihood of extreme autumn  
516 wildfire conditions across California, *Environ. Res. Lett.*, 15, 094016,  
517 <https://doi.org/10.1088/1748-9326/ab83a7>, 2020.

518

519 Guttikunda, S., and Nishadh, K. A.: Evolution of India's PM<sub>2.5</sub> pollution between 1998 and  
520 2020 using global reanalysis fields coupled with satellite observations and fuel  
521 consumption patterns, *Environ. Sci. Atmos.*, 2, 1502-1515,  
522 <https://doi.org/10.1039/D2EA00027J>, 2022.

523

524 Hoesly, R. M., Smith, S. J., Feng, L., Klimont, Z., Janssens-Maenhout, G., Pitkanen, T.,  
525 Seibert, J. J., Vu, L., Andres, R. J., Bolt, R. M., Bond, T. C., Dawidowski, L., Kholod,  
526 N., Kurokawa, J., Li, M., Liu, L., Lu, Z., Moura, M. C. P., O'Rourke, P. R., and Zhang,  
527 Q.: Historical (1750–2014) anthropogenic emissions of reactive gases and aerosols from  
528 the Community Emissions Data System (CEDS), *Geosci. Model Dev.*, 11, 369–408,  
529 <https://doi.org/10.5194/gmd-11-369-2018>, 2018.

530

531 Jaffe, D., Anderson, T., Covert, D., Kotchenruther, R., Trost, B., Danielson, J., Simpson, W.,  
532 Berntsen, T., Karlsdottir, S., Blake, D., Harris, J., Carmichael, G., and Uno, I.: Transport  
533 of Asian air pollution to North America, *Geophys. Res. Lett.*, 26, 711–714,  
534 <https://doi.org/10.1029/1999GL900100>, 1999.

535

536 Jolly, W. M., Cochrane, M. A., Freeborn, P. H., Holden, Z. A., Brown, T. J., Williamson, G.  
537 J., and Bowman, D. M. J. S.: Climate-induced variations in global wildfire danger from  
538 1979 to 2013, *Nat. Commun.*, 6, 7537, <https://doi.org/10.1038/ncomms8537>, 2015.

539

540 Li, C., McLinden, C., Fioletov, V., Krotkov, N., Carn, S., Joiner, J., Streets, D., He, H., Ren,  
541 X., Li, Z., and Dickerson, R.: India Is Overtaking China as the World's Largest Emitter  
542 of Anthropogenic Sulfur Dioxide, *Sci. Rep.*, 7, 14304, <https://doi.org/10.1038/s41598-017-14639-8>, 2017.

543

544

545 Li, H., Yang, Y., Wang, H., Li, B., Wang, P., Li, J., and Liao, H.: Constructing a  
546 spatiotemporally coherent long-term PM<sub>2.5</sub> concentration dataset over China using a  
547 machine learning approach, *Sci. Total Environ.*, 765, 144263,  
548 <https://doi.org/10.1016/j.scitotenv.2020.144263>, 2021.

549



550 Liao, H., Chang, W., and Yang, Y.: Climatic effects of air pollutants over China: A review,  
551 *Adv. Atmos. Sci.*, 32, 115–139, <https://doi.org/10.1007/s00376-014-0013-x>, 2015.

552

553 Lim, C.-H., Ryu, J., Choi, Y., Jeon, S. W., and Lee, W.-K.: Understanding global PM<sub>2.5</sub>  
554 concentrations and their drivers in recent decades (1998–2016), *Environ. Int.*, 144,  
555 106011, <https://doi.org/10.1016/j.envint.2020.106011>, 2020.

556

557 Lin, J., Pan, D., Davis, S. J., Zhang, Q., He, K., Wang, C., Streets, D. G., Wuebbles, D. J.,  
558 and Guan, D.: China’s international trade and air pollution in the United States, *Proc.*  
559 *Natl. Acad. Sci.*, 111, 1736–1741, <https://doi.org/10.1073/pnas.1312860111>, 2014.

560

561 Liu, J., and Mauzerall, D.: Estimating the average time for inter-continental transport of air  
562 pollutants, *Geophys. Res. Lett.*, 32, L11814, <https://doi.org/10.1029/2005GL022619>,  
563 2005.

564

565 Liu, J., Mauzerall, D. L., Horowitz, L. W., Ginoux, P., and Fiore, A. M.: Evaluating inter-  
566 continental transport of fine aerosols: (1) Methodology, global aerosol distribution and  
567 optical depth, *Atmos. Environ.*, 43, 4327–4338,  
568 <https://doi.org/10.1016/j.atmosenv.2009.03.054>, 2009.

569

570 Lohmann, U., and Feichter, J.: Global indirect aerosol effects: a review, *Atmos. Chem. Phys.*,  
571 5, 715–737, <https://doi.org/10.5194/acp-5-715-2005>, 2005.

572

573 Lou, S., Yang, Y., Wang, H., Smith, S. J., Qian, Y., and Rasch, P. J.: Black carbon amplifies  
574 haze over the North China Plain by weakening the East Asian winter monsoon,  
575 *Geophys. Res. Lett.*, 46, 452–460, <https://doi.org/10.1029/2018GL080941>, 2019.

576

577 Navinya, C. D., Vinoj, V. and Pandey, S. K.: Evaluation of PM<sub>2.5</sub> Surface Concentrations  
578 Simulated by NASA’s MERRA Version 2 Aerosol Reanalysis over India and its relation  
579 to the Air Quality Index, *Aerosol Air Qual. Res.*, 20, 1329–1339,  
580 <https://doi.org/10.4209/aaqr.2019.12.0615>, 2020.

581

582 Pöschl, U.: Atmospheric Aerosols: Composition, Transformation, Climate and Health  
583 Effects, *Angew. Chem. Int. Ed.*, 44, 7520–7540,  
584 <https://doi.org/10.1002/anie.200501122>, 2005.

585

586 Rasch, P. J., Xie, S., Ma, P.-L., Lin, W., Wang, H., Tang, Q., Burrows, S. M., Caldwell, P.,  
587 Zhang, K., Easter, R. C., Cameron-Smith, P., Singh, B., Wan, H., Golaz, J.-C., Harrop,  
588 B. E., Roesler, E., Bacmeister, J., Larson, V. E., Evans, K. J., Qian, Y., Taylor, M.,  
589 Leung, L. R., Zhang, Y., Brent, L., Branstetter, M., Hannay, C., Mahajan, S.,  
590 Mامتjanov, A., Neale, R., Richter, J. H., Yoon, J.-H., Zender, C. S., Bader, D.,  
591 Flanner, M., Foucar, J. G., Jacob, R., Keen, N., Klein, S. A., Liu, X., Salinger, A. G.,  
592 Shrivastava, M., and Yang, Y.: An overview of the atmospheric component of the

593 Energy Exascale Earth System Model, *J. Adv. Model. Earth Sy.*, 11, 2377–2411,  
594 <https://doi.org/10.1029/2019MS001629>, 2019.

595

596 Ren, L., Yang, Y., Wang, H., Wang, P., Chen, L., Zhu, J., and Liao, H.: Aerosol transport  
597 pathways and source attribution in China during the COVID-19 outbreak, *Atmos. Chem.*  
598 *Phys.*, 21, 15431–15445, <https://doi.org/10.5194/acp-21-15431-2021>, 2021.

599

600 Rosenfeld, D., Lohmann, U., Raga, G. B., Kulmala, M., Fuzzi, S., Reissell, A., and Andreae,  
601 M. O.: Flood or Drought: How Do Aerosols Affect Precipitation?, *Science*, 321, 1309–  
602 1313, <https://doi.org/10.1126/science.1160606>, 2008.

603

604 Singh, T., Matsumi, Y., Nakayama, T., Hayashida, S., Patra, P. K., Yasutomi, N., Kajino, M.,  
605 Yamaji, K., Khatri, P., Takigawa, M., Araki, H., Kurogi, Y., Kuji, M., Muramatsu, K.,  
606 Imasu, R., Ananda, A., Arbain, A. A., Ravindra, K., Bhardwaj, S., Kumar, S., Mor, S.,  
607 Dhaka, S. K., Dimri, A. P., Sharma, A., Singh, N., Bhatti, M. S., Yadav, R., Vatta, K.,  
608 and Mor, S.: Very high particulate pollution over northwest India captured by a high-  
609 density in situ sensor network, *Sci. Rep.*, 13, 13201, [https://doi.org/10.1038/s41598-023-](https://doi.org/10.1038/s41598-023-39471-1)  
610 [39471-1](https://doi.org/10.1038/s41598-023-39471-1), 2023.

611

612 Smith, S. J., van Aardenne, J., Klimont, Z., Andres, R. J., Volke, A., and Arias, S. D.:  
613 Anthropogenic sulfur dioxide emissions: 1850–2005, *Atmos. Chem. Phys.*, 11, 1101–  
614 1116, <https://doi.org/10.5194/acp-11-1101-2011>, 2011.

615

616 Stohl, A., and Trickl, T.: A textbook example of long-range transport: Simultaneous  
617 observation of ozone maxima of stratospheric and North American origin in the free  
618 troposphere over Europe, *J. Geophys. Res.*, 104, 30445–30462,  
619 <https://doi.org/10.1029/1999JD900803>, 1999.

620

621 Urdiales-Flores, D., Zittis, G., Hadjinicolaou, P., Osipov, S., Klingmüller, K., Mihalopoulos,  
622 N., Kanakidou, M., Economou, T., and Lelieveld, J.: Drivers of accelerated warming in  
623 Mediterranean climate-type regions, *npj. Clim. Atmos. Sci.*, 6, 97,  
624 <https://doi.org/10.1038/s41612-023-00423-1>, 2023.

625

626 van Marle, M. J. E., Kloster, S., Magi, B. I., Marlon, J. R., Daniau, A.-L., Field, R. D.,  
627 Arneth, A., Forrest, M., Hantson, S., Kehrwald, N. M., Knorr, W., Lasslop, G., Li, F.,  
628 Mangeon, S., Yue, C., Kaiser, J. W., and van der Werf, G. R.: Historic global biomass  
629 burning emissions for CMIP6 (BB4CMIP) based on merging satellite observations with  
630 proxies and fire models (1750–2015), *Geosci. Model Dev.*, 10, 3329–3357,  
631 <https://doi.org/10.5194/gmd-10-3329-2017>, 2017.

632

633 Wang, H., Rasch, P. J., Easter, R. C., Singh, B., Zhang, R., Ma, P.-L., Qian, Y., Ghan, S. J.,  
634 and Beagley, N.: Using an explicit emission tagging method in global modeling of  
635 source-receptor relationships for black carbon in the Arctic: Variations, sources, and

636 transport pathways, *J. Geophys. Res. Atmos.*, 119, 12888–12909,  
637 <https://doi.org/10.1002/2014JD022297>, 2014.

638

639 Wang, H., Easter, R. C., Zhang, R., Ma, P.-L., Singh, B., Zhang, K., Ganguly, D., Rasch, P.  
640 J., Burrows, S. M., Ghan, S. J., Lou, S., Qian, Y., Yang, Y., Feng, Y., Flanner, M.,  
641 Leung, L. R., Liu, X., Shrivastava, M., Sun, J., Tang, Q., Xie, S., and Yoon, J.-H.:  
642 Aerosols in the E3SM Version 1: New developments and their impacts on radiative  
643 forcing, *J. Adv. Model. Earth Syst.*, 12, e2019MS001851,  
644 <https://doi.org/10.1029/2019MS001851>, 2020.

645

646 Wang, P., Yang, Y., Xue, D., Ren, L., Tang, J., Leung, L. R., and Liao, H.: Aerosols overtake  
647 greenhouse gases causing a warmer climate and more weather extremes toward carbon  
648 neutrality, *Nat. Commun.*, 14, 7257, <https://doi.org/10.1038/s41467-023-42891-2>, 2023.

649

650 Wang, Y., Liu, X., Hoose, C., and Wang, B.: Different contact angle distributions for  
651 heterogeneous ice nucleation in the Community Atmospheric Model version 5, *Atmos.*  
652 *Chem. Phys.*, 14, 10411–10430, <https://doi.org/10.5194/acp-14-10411-2014>, 2014.

653

654 Yang, Y., Wang, H., Smith, S. J., Easter, R., Ma, P.-L., Qian, Y., Yu, H., Li, C., and Rasch,  
655 P. J.: Global source attribution of sulfate concentration and direct and indirect radiative  
656 forcing, *Atmos. Chem. Phys.*, 17, 8903–8922, [https://doi.org/10.5194/acp-17-8903-](https://doi.org/10.5194/acp-17-8903-2017)  
657 [2017](https://doi.org/10.5194/acp-17-8903-2017), 2017.

658

659 Yang, Y., Wang, H., Smith, S. J., Zhang, R., Lou, S., Qian, Y., Ma, P., and Rasch P. J.:  
660 Recent intensification of winter haze in China linked to foreign emissions and  
661 meteorology, *Sci. Rep.*, 8, 2107, <https://doi.org/10.1038/s41598-018-20437-7>, 2018a.

662

663 Yang, Y., Wang, H., Smith, S. J., Zhang, R., Lou, S., Yu, H., Li, C., and Rasch, P. J.: Source  
664 Apportionments of Aerosols and Their Direct Radiative Forcing and Long-Term Trends  
665 Over Continental United States, *Earth's Future*, 6, 793–808,  
666 <https://doi.org/10.1029/2018EF000859>, 2018b.

667

668 Yang, Y., Ren, L., Li, H., Wang, H., Wang, P., Chen, L., Yue, X., and Hong, L.: Fast climate  
669 responses to aerosol emission reductions during the COVID-19 pandemic, *Geophys.*  
670 *Res. Lett.*, 47, e2020GL089788, <https://doi.org/10.1029/2020GL089788>, 2020a.

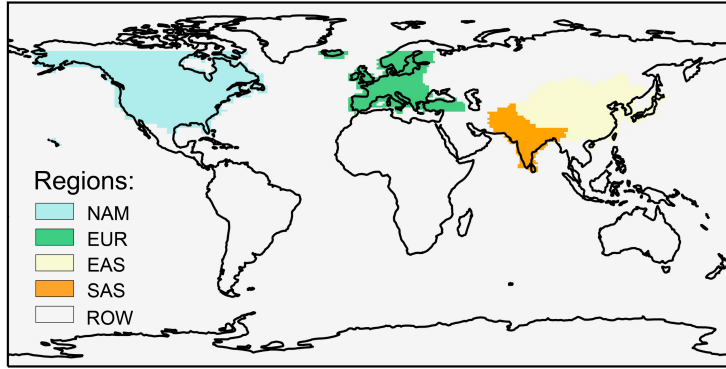
671

672 Yang, Y., Lou, S., Wang, H., Wang, P., and Liao, H.: Trends and source apportionment of  
673 aerosols in Europe during 1980–2018, *Atmos. Chem. Phys.*, 20, 2579–2590,  
674 <https://doi.org/10.5194/acp-20-2579-2020>, 2020b.

675

676 Yang, Y., Ren, L., Wu, M., Wang, H., Song, F., Leung, L. R., Hao, X., Li, J., Chen, L., Li,  
677 H., Zeng, L., Zhou, Y., Wang, P., Liao, H., Wang, J., and Zhou, Z.-Q.: Abrupt emissions  
678 reductions during COVID-19 contributed to record summer rainfall in China, *Nat.*  
679 *Commun.*, 13, 959, <https://doi.org/10.1038/s41467-022-28537-9>, 2022a

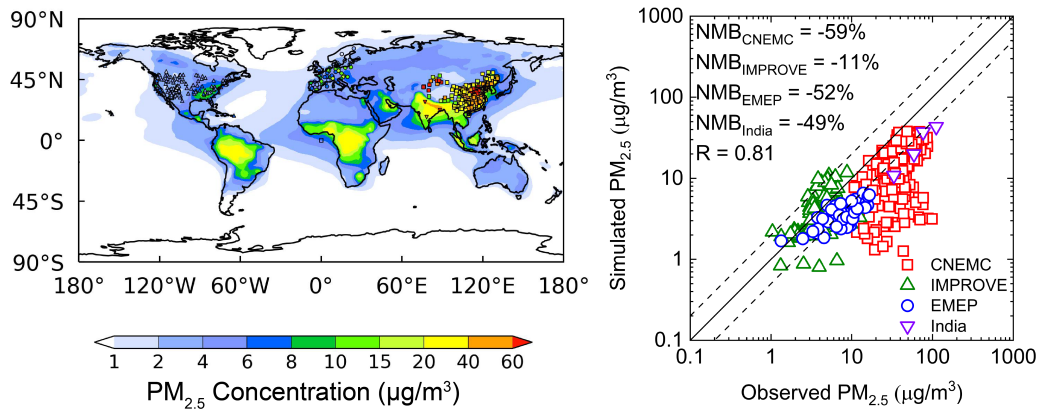
680  
681 Yang, Y., Zeng, L., Wang, H., Wang, P., and Liao, H.: Dust pollution in China affected by  
682 different spatial and temporal types of El Niño, *Atmos. Chem. Phys.*, 22, 14489–14502,  
683 <https://doi.org/10.5194/acp-22-14489-2022>, 2022b.  
684  
685 Yang, Y., Zeng, L., Wang, H., Wang, P., and Liao, H.: Climate effects of future aerosol  
686 reductions for achieving carbon neutrality in China, *Sci. Bull.*, 68, 902–905,  
687 <https://doi.org/10.1016/j.scib.2023.03.048>, 2023..  
688  
689 Zeng, L., Yang, Y., Wang, H., Wang, J., Li, J., Ren, L., Li, H., Zhou, Y., Wang, P., and Liao,  
690 H.: Intensified modulation of winter aerosol pollution in China by El Niño with short  
691 duration, *Atmos. Chem. Phys.*, 21, 10745–10761, [https://doi.org/10.5194/acp-21-10745-](https://doi.org/10.5194/acp-21-10745-2021)  
692 [2021](https://doi.org/10.5194/acp-21-10745-2021), 2021.  
693  
694 Zhang, Q., Jiang, X., Tong, D., Davis, S. J., Zhao, H., Geng, G., Feng, T., Zheng, B., Lu, Z.,  
695 Streets, D. G., Ni, R., Brauer, M., van Donkelaar, A., Martin, R. V., Huo, H., Liu, Z.,  
696 Pan, D., Kan, H., Yan, Y., Lin, J., He, K., and Guan, D.: Transboundary health impacts  
697 of transported global air pollution and international trade, *Nature*, 543, 705–709,  
698 <https://doi.org/10.1038/nature21712>, 2017.  
699  
700 Zheng, B., Tong, D., Li, M., Liu, F., Hong, C., Geng, G., Li, H., Li, X., Peng, L., Qi, J., Yan,  
701 L., Zhang, Y., Zhao, H., Zheng, Y., He, K., and Zhang, Q.: Trends in China’s  
702 anthropogenic emissions since 2010 as the consequence of clean air actions, *Atmos.*  
703 *Chem. Phys.*, 18, 14095–14111, [https://doi.org/10.5194/acp-18-14095-](https://doi.org/10.5194/acp-18-14095-2018)  
704 [2018](https://doi.org/10.5194/acp-18-14095-2018), 2018.



705

706 **Figure 1.** Tagged source regions (NAM: North America; EUR: Europe; EAS: East Asia; SAS:

707 South Asia; ROW: rest of the world).



708

709

710

711

712

713

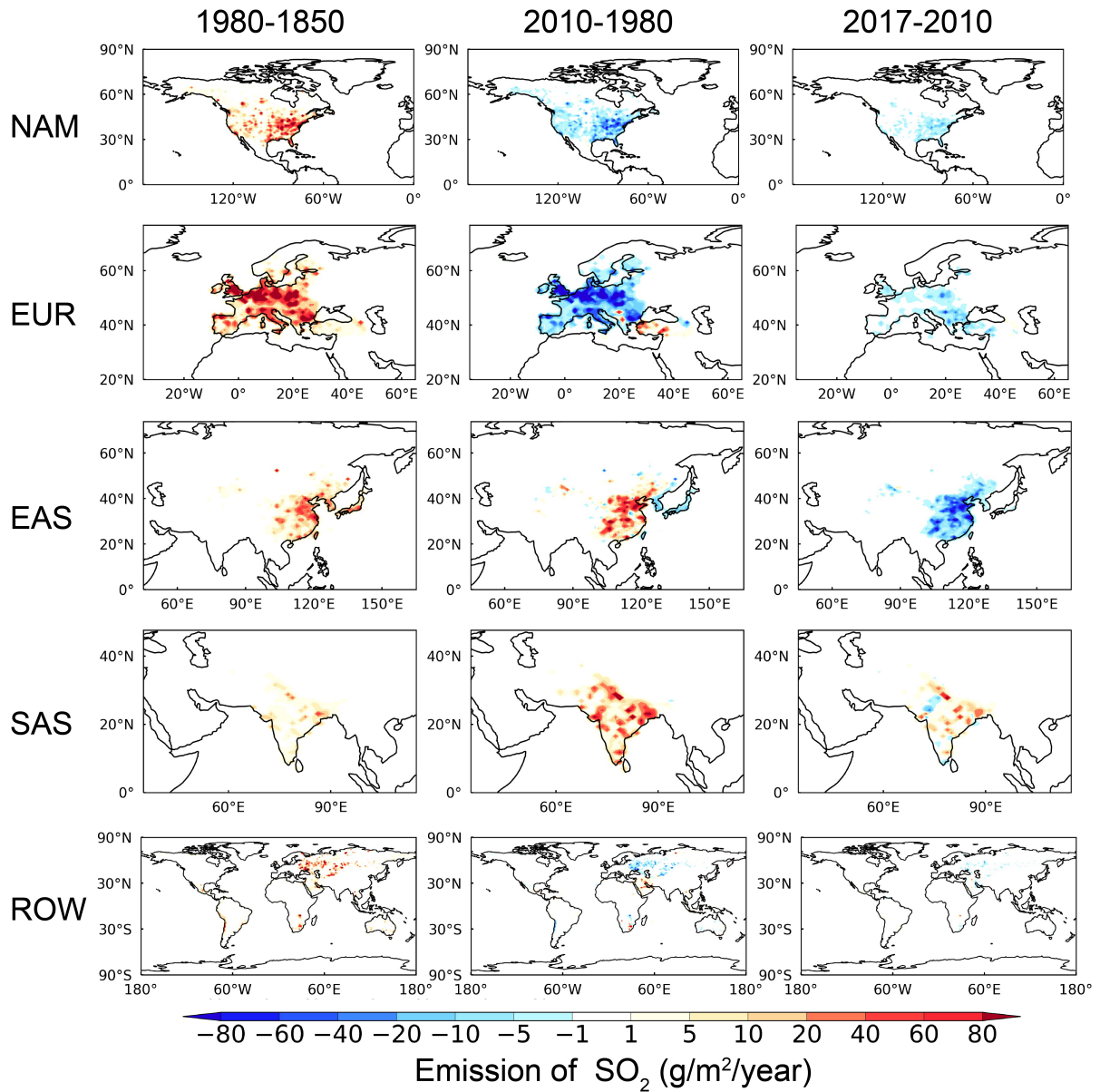
714

715

716

717

**Figure 2.** Spatial distribution (left panel) and scatter plot (right) between the simulated and observed annual mean near-surface  $PM_{2.5}$  concentrations ( $\mu g/m^3$ ) in 2017. Observational data are from IMPROVE (triangle), EMEP (circle), India (inverted triangle) and CNEMC (square). The solid line marks the 1:1 ratio and dashed lines mark the 1:2 and 2:1 ratios. Normalized mean bias (NMB) and correlation coefficient (R) between observation and simulation are shown on the right panel.  $NMB = 100\% \times \sum(M_i - O_i) / \sum O_i$ , where  $M_i$  and  $O_i$  are the modeled and observed values at site  $i$ , respectively.

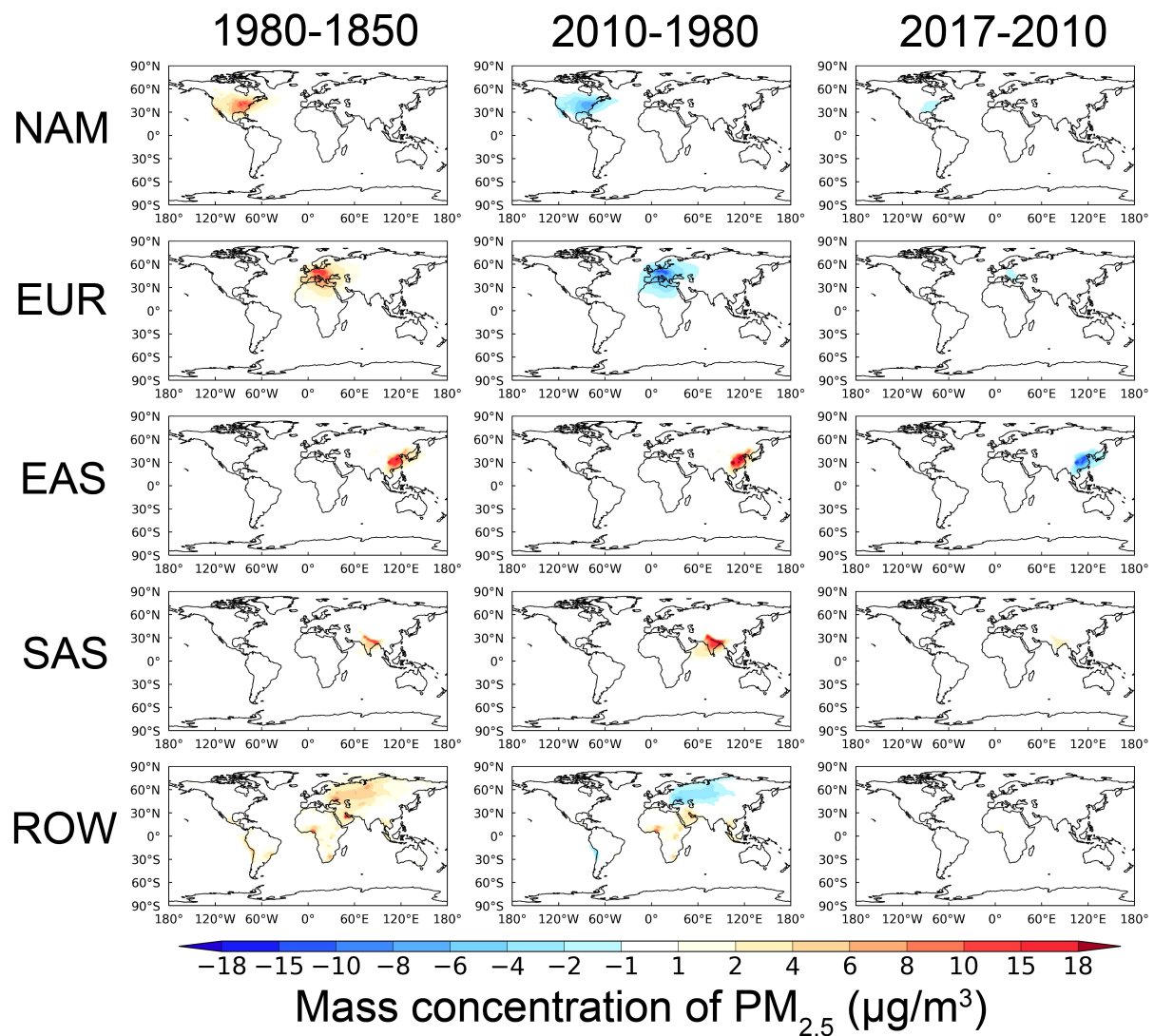


718

719 **Figure 3.** Changes in anthropogenic sulfur dioxide (SO<sub>2</sub>) emissions (g/m<sup>2</sup>/year) between 1850  
 720 and 1980 (left), between 1980 and 2010 (middle), and between 2010 and 2017 (right) in the 5  
 721 tagged source regions (NAM, EUR, EAS, SAS and ROW from top to bottom).

722

723

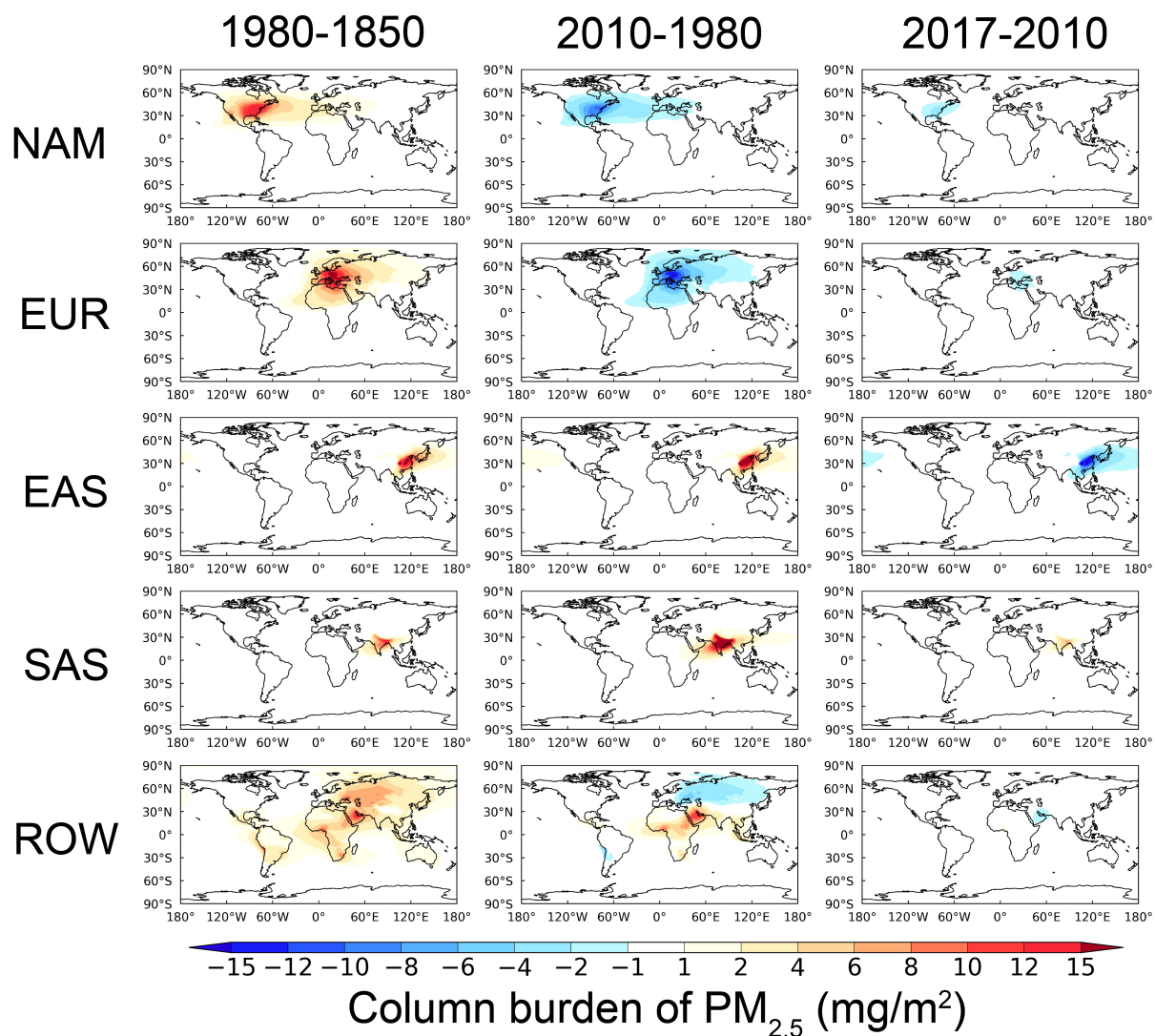


724

725 **Figure 4.** Changes in near-surface mass concentration ( $\mu g/m^3$ ) of anthropogenic  $PM_{2.5}$   
 726 contributed by the 5 tagged source regions (NAM, EUR, EAS, SAS and ROW from top to  
 727 bottom) between 1850 and 1980 (left), between 1980 and 2010 (middle), and between 1980  
 728 and 2017 (right).

729

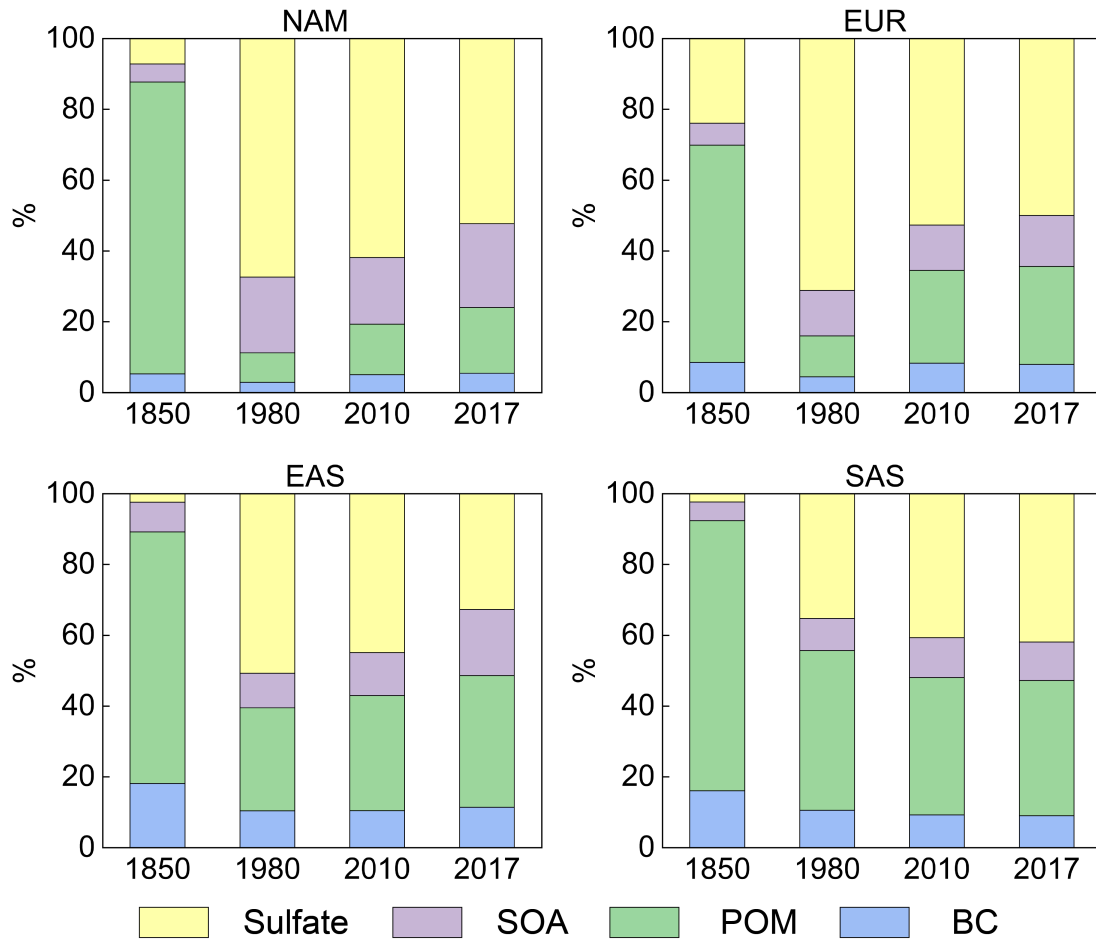




730

731 **Figure 5.** Changes in column burden (mg/m<sup>2</sup>) of anthropogenic PM<sub>2.5</sub> contributed by the 5  
 732 tagged source regions (NAM, EUR, EAS, SAS and ROW from top to bottom) between 1850  
 733 and 1980 (left), between 1980 and 2010 (middle), and between 2010 and 2017 (right).

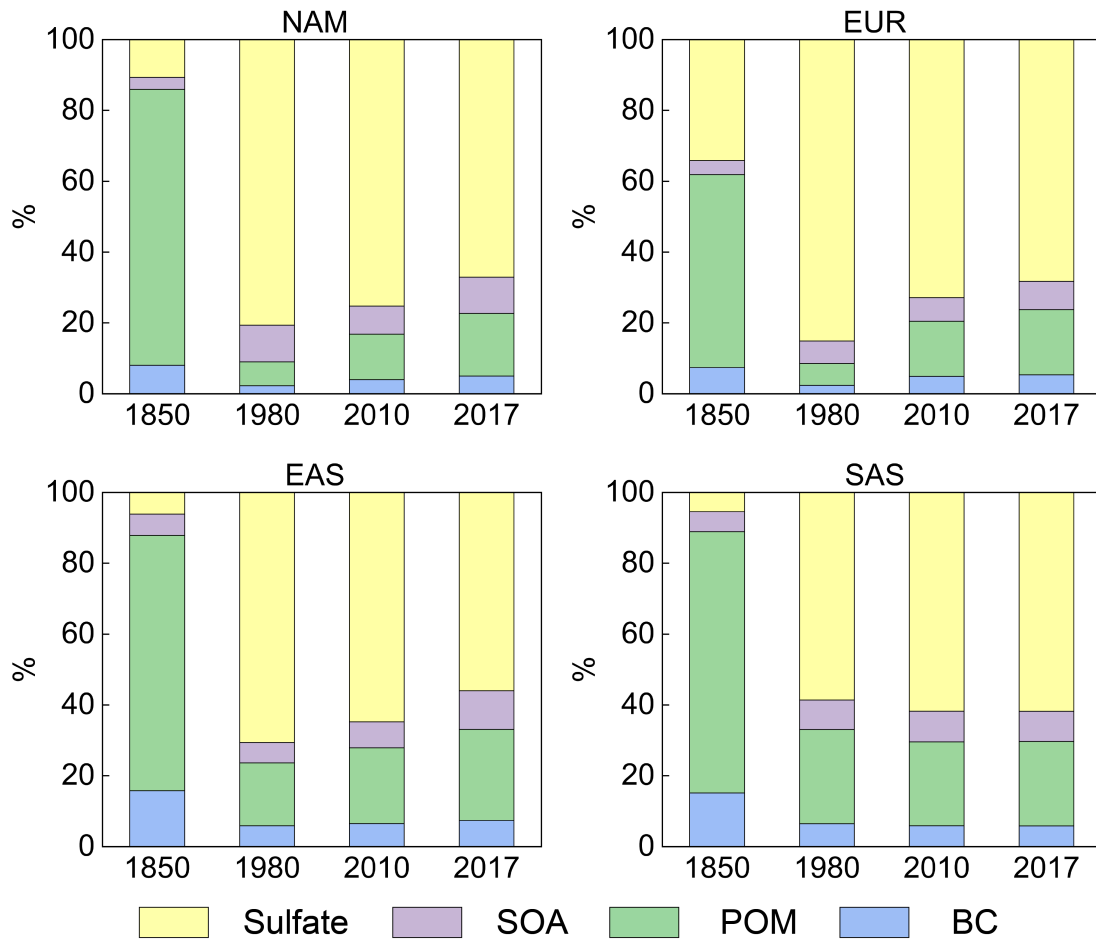
734



735

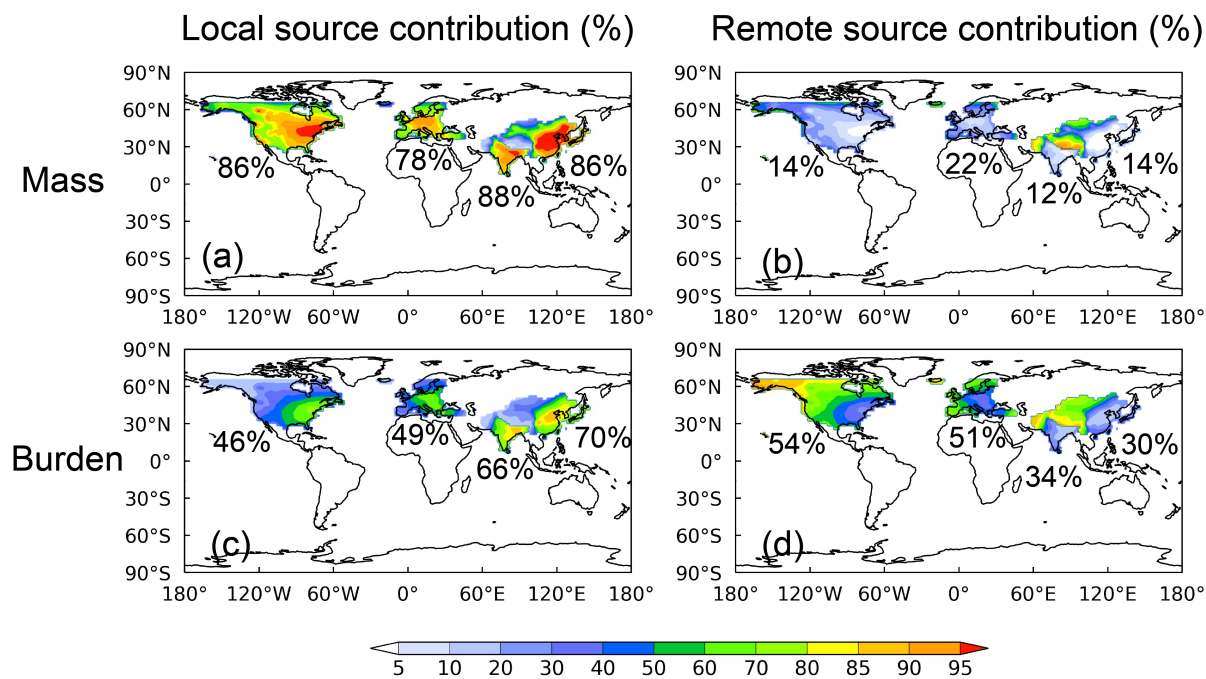
736 **Figure 6.** Percentage contributions (%) of aerosol species including BC, POM, SOA and  
 737 sulfate to the near-surface mass concentrations of PM<sub>2.5</sub> averaged over the four major emission  
 738 source regions (NAM, EUR, EAS and SAS) in the focused four years (1850, 1980, 2010 and  
 739 2017).

740



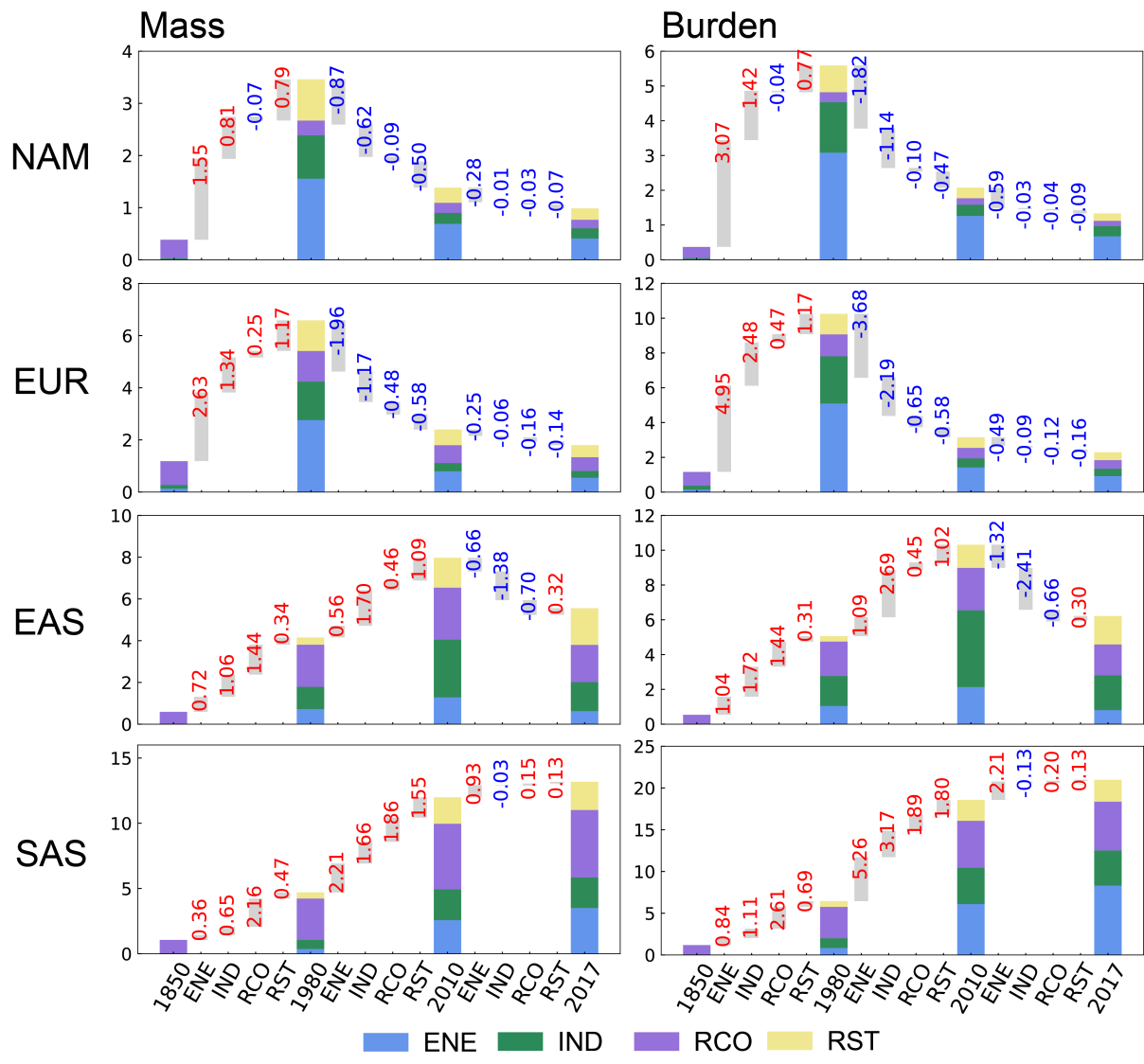
741

742 **Figure 7.** Percentage contributions (%) of aerosol species including BC, POM, SOA and  
 743 sulfate to the column burden of PM<sub>2.5</sub> averaged over the four major emission source regions  
 744 (NAM, EUR, EAS and SAS) in the focused four years (1850, 1980, 2010 and 2017).  
 745



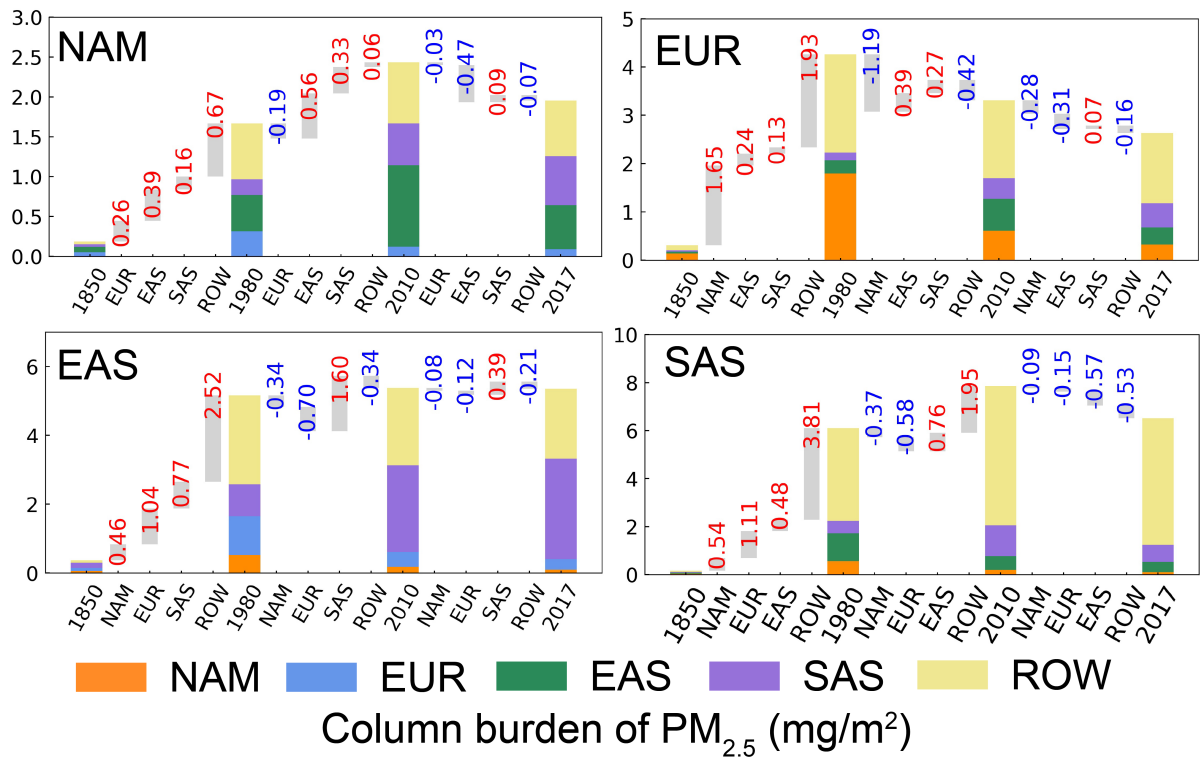
746

747 **Figure 8.** Relative contributions (%) from (a, c) local and (b, d) remote anthropogenic  
 748 emissions to the near-surface mass concentrations and column burdens of PM<sub>2.5</sub> in the four  
 749 targeted regions (NAM, EUR, EAS and SAS) in 2010. Numbers marked on the figure are the  
 750 regional average over the four individual targeted regions.  
 751



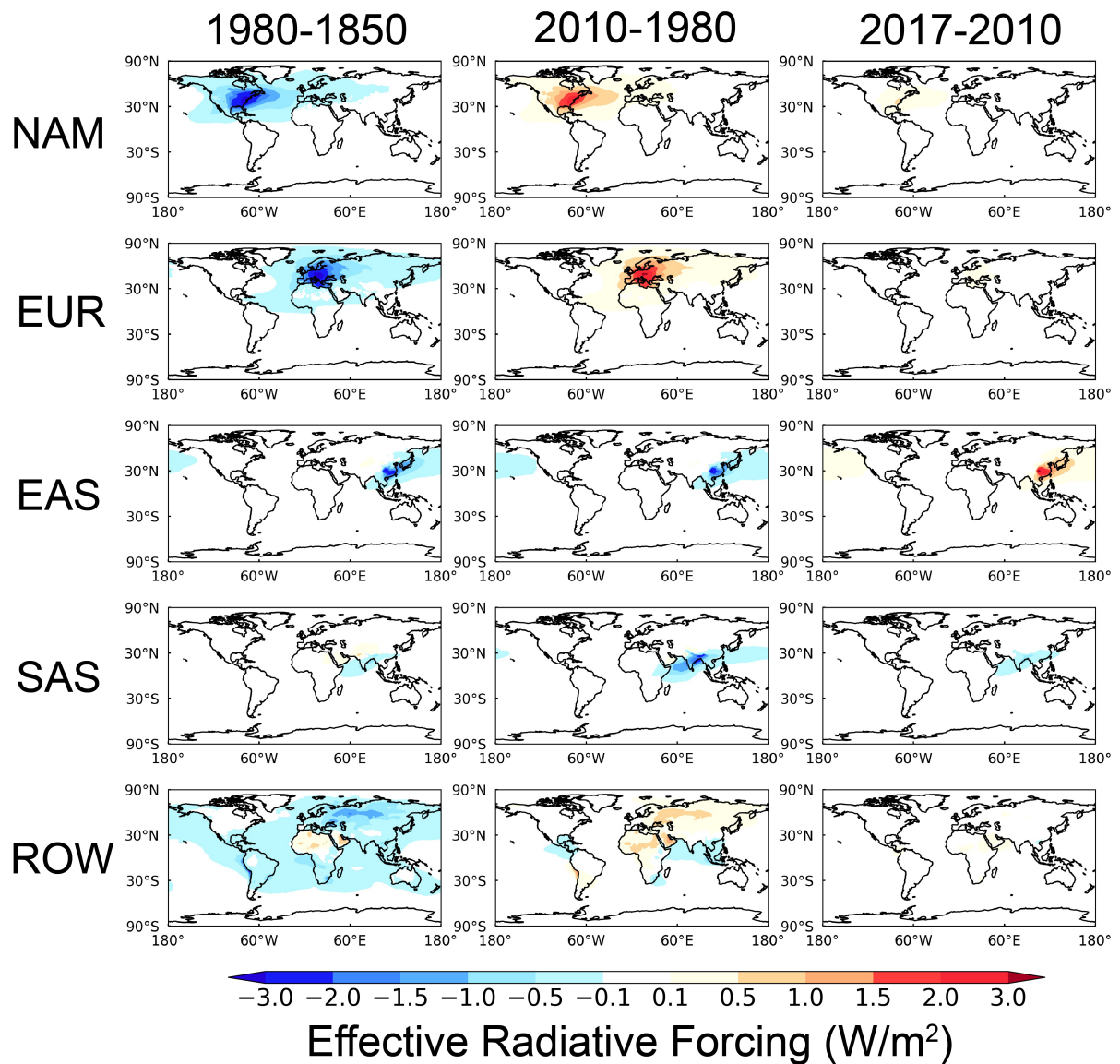
752  
753  
754  
755  
756  
757  
758  
759

**Figure 9.** Local source contributions from four individual emission sectors (ENE, IND, RCO and RST) to the near-surface mass concentrations ( $\mu\text{g}/\text{m}^3$ , left) and column burdens ( $\text{mg}/\text{m}^2$ , right) of anthropogenic  $\text{PM}_{2.5}$  in the four targeted regions (NAM, EUR, EAS and SAS from top to bottom) for years 1850, 1980, 2010 and 2017 (in color bars). Grey bar and numbers between two years show the change in sector contributions. Positive values are shown in red and negative values are shown in blue.



760  
761  
762  
763  
764

**Figure 10.** Same as Figure 9, but for contributions from the remote tagged source regions to the column burdens (mg/m<sup>2</sup>) of anthropogenic PM<sub>2.5</sub> in the four targeted regions (NAM, EUR, EAS and SAS).



765  
 766 **Figure 11.** Changes in effective radiative forcing ( $W m^{-2}$ ) at the top of the atmosphere due to  
 767 aerosol-radiation interactions between 1850 and 1980 (left), between 1980 and 2010 (middle),  
 768 and between 2010 and 2017 (right) attributed to the changes in anthropogenic emissions from  
 769 NAM, EUR, EAS, SAS and ROW (from top to bottom).